

An Open Framework to Model Diffraction by Dynamic Blockers in Millimeter Wave Simulations

Paolo Testolina, Mattia Lecci, Alessandro Traspadini, and Michele Zorzi

Department of Information Engineering, University of Padova, Italy

E-mail: {testolina, leccimat, traspadini, zorzi}@dei.unipd.it

Abstract—The millimeter wave (mmWave) band will be exploited to address the growing demand for high data rates and low latency. The higher frequencies, however, are prone to limitations on the propagation of the signal in the environment. Thus, highly directional beamforming is needed to increase the antenna gain. Another crucial problem of the mmWave frequencies is their vulnerability to blockage by physical obstacles. To this aim, we studied the problem of modeling the impact of second-order effects on mmWave channels, specifically the susceptibility of the mmWave signals to physical blockers. With respect to existing works on this topic, our project focuses on scenarios where mmWaves interact with multiple, dynamic blockers. Our open source software includes diffraction-based blockage models and interfaces directly with an open source Radio Frequency (RF) ray-tracing software.

Index Terms—5G, millimeter wave networks, simulation, channel model, diffraction, propagation.

I. INTRODUCTION

The millimeter wave (mmWave) frequencies feature large chunks of untapped bandwidth that can increase the data rate provided to the end users, and the small wavelength enables the design of antenna arrays with tens of elements in a small form factor to support beamformed transmissions. While these promising characteristics make the mmWave technology able to meet the requirements of 5th generation (5G) cellular systems and Wi-Fi networks [1], [2], there are several concerns regarding the propagation characteristics at these frequencies that justify a more accurate study and the need for new channel models. First, the high propagation loss limits the coverage region of mmWave base stations, although large antenna arrays and complex beamforming techniques can mitigate the problem. Second, at mmWaves, the increased diffraction loss results in deep shadow regions, thus further degrading the communications performance [3], [4]. Furthermore, mmWave signals can be easily blocked by obstacles (e.g., vehicles, buildings, vegetation, human bodies), which may prevent direct Line-of-Sight (LoS) communications. These (often unpredictable) propagation components make it imperative to accurately model the dynamics of the surrounding environment, and to design communication protocols, and especially beam-tracking algorithms, taking into account these disruptive events.

In this context, ray tracing has emerged as an essential tool to model the mmWave channel [5], especially, but not limited to, when detailed link-level protocols need to be simulated. With respect to stochastic channel models, ray tracers

(RTs) exploit a digital reconstruction of the environment to achieve a greater degree of accuracy, at the cost of additional computational load [6]. Generally, the digital model includes the static elements of the scenario, e.g., the floor, ceiling and walls, and the tables, screens and other objects, depending on its level of detail. Its design is not trivial, as it requires the use of a Computer-Aided Design (CAD) software, a complex and time-consuming task. Furthermore, dynamic elements, e.g., moving humans and vehicles, are not generally considered, as their movements can not be included in a single CAD file. Thus, these elements are often overlooked in RT simulations, despite the significant role they play in the propagation of the signal [7], [8]. Furthermore, the study of the impact of blockers on the network performance has been limited to ad hoc scenarios, often considering a single blocker and only at the PHY layer. On the contrary, their effect on large-scale, high-level network simulations has not yet been fully characterized, due to the complexity of designing the scenario and modeling the diffraction when considering moving obstacles.

In this work, we present the *Blockage Manager*¹, a novel open-source software to model dynamic blockers in RT simulations. The application was designed to post-process information typically obtained from RT software, offering the user a simple yet powerful interface to introduce blockage models on top of them, making their simulations more realistic and dynamic. Starting from a pre-processed simulation allows the user to later add as many obstacles as desired, with custom mobility and settings, without the need to run an entirely new ray-tracing simulation from scratch, which can take a significant amount of time. The software has been designed to present as simple an API as possible, so that the user only has to create a high-level description of the desired obstacles, while still having some control on fine-tuning parameters if desired, and leaving all the complexity to the simulator.

The aim of this work is to describe an open-source software able to (i) interface directly with *qd-realization* [9], an open-source RF ray-tracing software, importing and exporting channel traces with a single line of code, (ii) process pre-computed RT simulations, adding multiple mobile obstacles on top of them, (iii) support already implemented blockage models, with varying degrees of complexity and accuracy. Furthermore, we showcase some basic network scenarios processed with our *Blockage Manager*, describing the obtained results and discussing future works that will enable it to closely mimic real channel behaviors in the presence of

¹The *Blockage Manager* is available at <https://github.com/signetlabdei/rt-blockage-manager>.

This work was partially supported by the National Institute of Standards and Technology (NIST) under award no. 60NANB20D082. The work of M. Lecci and P. Testolina was supported by Fondazione CaRiPaRo under grants "Dottorati di Ricerca" 2018 and 2019.

obstacles, allowing the community to better study and design link-level protocols for mmWave communications.

In the remainder of the paper, we first report the state of the art on diffraction modeling (Sec. II). Then, Sec. III offers a brief overview of the framework architecture, giving the essential details to understand its main components. In Sec. IV, we present the blockage models that are currently implemented in the framework. Finally, the results in Sec. V serve the double purpose of showcasing the usage of the *Blockage Manager* and of highlighting the impact of dynamic blockage in mmWave networks, and Sec. VI presents some concluding remarks and future work directions.

II. STATE OF THE ART

Signals at mmWave frequencies are prone to limitations on their propagation in the environment. Therefore, understanding and precisely characterizing the interaction between radio waves and the surroundings is fundamental to characterize communications in different scenarios.

This reason has led to different modeling approaches for the mmWave channel, which have various degrees of complexity and accuracy, and can be applied to different contexts and evaluations [6]. Thus, channel models can be summarized in: analytical, stochastic, and Quasi Deterministic (QD).

Analytical channel models: These models generally offer a simplified representation of the channel, based on propagation loss and a random variable representing fading. This kind of model has a limited accuracy and can be used to characterize communications in a generic environment [10]–[12], without accounting for the features of specific scenarios and their interaction with the elements typical of mmWave propagation (e.g., realistic antenna arrays and beamforming).

Stochastic channel models: They derive the entries of the channel matrix from a set of random distributions, whose parameters are determined by statistical fits on channel measurements for a generic scenario (e.g., a common rural or urban environment). Their speed and their stochastic nature allow to easily generate the radio channels for generic, large-scale scenarios. Models of this type, e.g., the one proposed in 3GPP TR 38.901 [13], have been used in the performance evaluations of mmWave networks [14], [15].

Quasi-Deterministic channel models: QD channels, instead, can accurately model the interactions of the mmWave signal with a specific environment [16]–[18]. However, since the Multi Path Components (MPCs) are generated by the interaction between the transmitted signal and the elements of a given environment, they can offer improved accuracy at the cost of a higher processing load.

Including the effect of blockage on the channel model is a non-trivial task. The high-level, generic nature of the analytical models makes it difficult to model the blockage by multiple, possibly moving obstacles (e.g., people, vehicles, foliage, etc.). Similarly, since stochastic channel models do not require a model of the propagation environment, it is difficult to define a temporally and spatially consistent behavior of the blockers. Furthermore, modeling specific mobility patterns does not agree well with the stochastic nature of the channel, and can decrease the advantages of these kinds of models (i.e., their being lightweight and easy to use). Finally, as mentioned in Sec. I, placing (possibly dynamic) blockers in an RT simulation can also be challenging, thus motivating this work. In the remainder of this section, we present the

existing models in the literature that deal with this problem. Namely, we first report the main works on blockage at the channel modeling level, and then its modeling at the higher layers of the network stack.

The authors of [19] analyzed the scattering of a vehicle and showed that RT simulations of complex objects allow the derivation of simplified scattering models. This is fundamental, since only by reducing the complexity of large objects does it become possible to simulate realistic scenarios. Their results show that, rather than introducing a complex model with a high polygon count, it is possible to reduce the complexity of simulations involving cars by only considering a few key points producing scattering, e.g., wing mirrors.

Another simplification was described also for human blockage in [20], where the authors analyzed their measurements taken at 10.5 GHz and concluded that a metal cylinder affects the radio channel similarly to a human body. This result justifies the usage of such a simple model in practical simulations rather than modeling a detailed person, a significantly harder task to perform with a correspondingly much higher computational cost.

The 3GPP also proposes a map-based hybrid channel model [13] using [21] for the deterministic component of the channel, and adding a random component to model clusters of MPCs. It also proposes the usage of two blockage models, to better represent a dynamic and realistic channel. In the stochastic blockage model (Blockage model A), random rectangular regions are blocked, considering the temporal and spatial correlation for completeness. The geometric blockage model (Blockage model B) deploys rectangular screens, specifying their relative dimensions and mobility patterns. In both cases, a Knife-Edge Diffraction (KED) at four edges is defined, using the arctan approximation, described in Sec. IV, for the diffraction loss.

A low-complexity enhancement of this approximation was studied in [22] using a Fourier-based model for human obstacles. Its authors compared their simulations with measurements at 2.44 GHz in an indoor Non-Line-of-Sight (NLoS) scenario and showed that their approximation produces shadowing loss closer to the Fresnel formulas for Double Knife-Edge Diffraction (DKED) than the simpler arctan model.

Besides, the validity of the KED model was proved for narrow obstacles also using complex specific solvers for Maxwell's equations as described in [23].

A series of modifications and criteria to improve the accuracy of the 3GPP model are provided in [24]. It proposed, in case of multiple blockers in close proximity, to consider them as a single blocker with increased size. The authors also suggest a way to increase the accuracy when the transmitted beam does not cover the entire obstacle surface, for instance, when highly directional antennas at a relative short distance are employed. In such cases, the idea consists of taking into consideration the transmitted beam pattern to choose the position of the diffraction points on the surface of the obstacles. A measurement campaign was carried out, and its results showed that with these modifications the loss prediction provided by the 3GPP model can be improved.

The literature also includes some studies analyzing blockage experimentally [7], [8], [25]. The authors in [7] analyzed accurate measurements of human body blockage at 60 GHz with a person that traversed a linear trajectory perpendicular to the direct path between the Transmitter (TX) and the

Receiver (RX). They derived a diffraction model and compared it with their measurements. Eventually, they showed that when a human obstacle is close to the path of the direct ray, it also creates a strong reflected ray, thus acting as a 2-ray propagation model.

A similar scenario was studied in [8] at 73 GHz. Its analysis showed that the use of directive antennas has a crucial impact on human blockage measurement results, especially when the blocker was close either to the TX or to the RX.

Furthermore, [26] explores the impact of human blockage on the channel model specifically proposed for IEEE 802.11ad [27], based on measurements at 60 GHz. Its authors analyzed ray tracing simulations in a human blockage scenario considering also diffraction effects. They found that the impact of human blockage is twofold. First of all, the Signal-to-Noise Ratio (SNR) at the RX decreases due to the additional attenuation, even if smart antennas are employed. On the other hand, the delay spread and the frequency selectivity in general increase, because the channel conditions change from LoS to NLoS. Both effects deteriorate the link, causing a higher bit error probability during communications.

The modern literature not only provides examples of works studying blockage at mmWaves from a physical measurement and modeling perspective, but also recognizes it as an issue that mmWave communication protocols need to address. In fact, while high frequencies are in principle capable of delivering the exceptional performance that they promise, they are also heavily affected by bad channel conditions, making the system much less stable thus worsening the Quality of Experience (QoE).

An analysis of blockage was performed in [25] to evaluate the effect of blockers on an End-to-End (E2E) application. The authors used a phased array system that measured the channel in multiple directions, in order to fully understand the path diversity.

Different analyses on Transmission Control Protocol (TCP) [28]–[31], studying the behavior of this protocol at mmWave frequencies, employed obstacles to simulate NLoS scenarios. Indeed, the extreme variability of the signal quality over mmWave links yields either degraded TCP goodput and very low utilization of the resources at mmWave frequencies, or, in the presence of link-layer retransmissions, high goodput at the price of high latency. Therefore, especially at mmWaves, the effect of obstacles is crucial to understand the actual condition of the channel.

As blockage is so impactful, especially on TCP-based communications, some works have proposed and tested ways of relying on multiple simultaneous connections, on both high and low frequencies, to balance resilience and raw throughput. Protocols such as Multipath TCP (MPTCP) have been analyzed [31]–[36], showing their advantages when, for example, buildings block the direct mmWave path or fast mobility cannot be fully supported by the mmWave network.

In [29], the authors assessed the goodput of a scenario in which obstacles of different sizes are placed in the area between the TX and the RX. The application layer simulated a file transfer with full buffer and the authors noticed that the number of obstacles plays a major role in the achievable goodput. With fewer obstacles, there is a higher probability of having a LoS channel and this has a crucial impact on the data rate available at the physical layer.

Thus, the use of more accurate channel models, modeling

for instance the diffraction effect of obstacles and considering appropriately the presence of multiple blockers, can provide more precise results. For example, even in a simple human blockage scenario where an obstacle moves perpendicularly to the line between the TX and the RX, the loss is higher when the obstacle crosses the LoS closer to one of the nodes. This phenomenon, shown in our simulations, can be described only by taking into account the diffraction effect of the obstacles. Thus, it can be easily understood that in more complex scenarios with many obstacles this effect has a critical impact on results. This is the reason why we implemented an open source software able to (i) include diffraction-based blockage models, (ii) interface directly with an open source Radio Frequency (RF) ray-tracing software, (iii) support multiple mobile blockers.

III. SOFTWARE ARCHITECTURE

The *Blockage Manager* was designed as a self-contained software to model the effect of blockage in RT traces. Doing it in post-processing allows running the computationally-demanding RT only once, including in the simulation all the static elements with a single CAD model. Any distribution of the dynamic elements, i.e., blockers, can then be introduced in the static scenario using the *Blockage Manager*, that can use the same RT output as a static baseline for any blocker configuration.

The *Blockage Manager* is organized in modules, each providing a set of classes and functions to handle the elements required for the simulation. Here, we report a brief overview of the different modules, to offer some insights on the implementation and to clarify how the results presented in Sec. V were obtained.

Although geometry libraries exist in Python [37], [38], in order to meet all the simulation requirements (3D geometry with fast computation time), and to build a self-contained package, we decided to implement all the basic geometrical objects and operations from scratch. Thus, we developed a custom `Geometry` module to handle the geometry of the ray and of the obstacles themselves, and to define consistent mobility patterns of the latter. This module underlies most of the operations carried out during the simulation and can be optimized independently in the future, thanks to the common object interface.

The RT traces can be imported in the *Blockage Manager* using the `Scenario` interface, that defines common methods to import/export traces in the target format, as well as to access and update sets of rays between nodes. Currently, the `Scenario` interface supports traces from the *qd-realization* software, which is specifically able to handle channel traces for multiple users and timesteps. However, the interface allows for the possibility to support different ray-tracing formats, that could be implemented in the future. The information for each ray (delay, path gain, phase, path) is stored in a `Ray` object, that also offers a simple interface to consistently compute Angles of Departure (AoDs) and Angles of Arrival (AoAs).

Then, blockers can be introduced in the scenario with the common `Obstacle` interface, that handles obstructions, diffraction, and other effects that a generic obstacle may impose over the Rays of the imported `Scenario`. Currently, a sphere, a rectangular and an *orthogonal-rectangular* screens

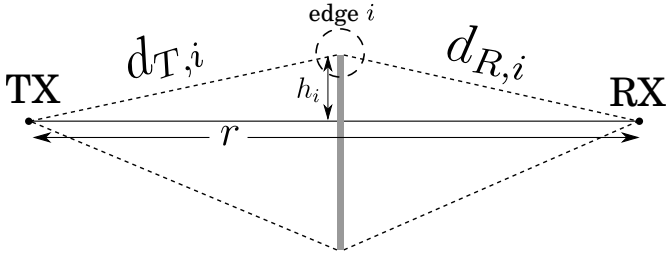


Fig. 1: DKED geometry.

are implemented. We defined the orthogonal-rectangular obstacle as an ideal rectangular screen that behaves as if it were orthogonal to any considered ray, when computing the interaction between the two. As detailed in Sec. IV, this artificial obstacle was introduced to meet the hypotheses of several diffraction models, that could thus be included in the software. On the contrary, the rectangular screen can be tilted in both the azimuth and elevation directions, thus providing a more general obstacle mobility at the cost of a limited set of available diffraction models. The movement of an obstacle during the simulation is described by a *MobilityModel*. At each time step, the position of each obstacle is updated based on such model, thereby providing accurate and temporally-correlated mobility and making the channel temporally consistent. The whole simulation, i.e., computing the interactions of the rays with the obstacles, and updating the positions of the obstacles at each time step, is handled by the *Environment*, that constitutes the core of the software, with just a few lines of code.

IV. BLOCKAGE MODELS

When considering the interaction between an object and a signal propagating in the free space from point T to point R , the Fresnel Zones offer a useful model to analyze the intensity of the diffraction. The Fresnel zones are concentric ellipses with focal points at T and R , and radius

$$r_n = \sqrt{n\lambda \frac{d_T d_R}{d_T + d_R}} \quad (1)$$

where λ is the wavelength of the transmitted signal, d_T (d_R) is the distance between the diffraction point and the transmitter (receiver), and n is the order of the Fresnel Zone. If the cross section of the First Fresnel Zone is obstructed, diffraction becomes the dominant term in the interaction with the object, with significant impact on the communication performance. In the *Blockage Manager*, several models to describe the diffraction loss are available. In this section, we provide a brief overview of those that were considered for the simulations described in Sec. V.

As the majority of the diffraction models is based on the Fresnel formulation, we define the complex Fresnel integral as:

$$F(\nu) = \int_0^\nu e^{j\frac{\pi s^2}{2}} ds \quad (2)$$

where ν is the Fresnel-Kirchhoff diffraction parameter:

$$\nu(h) = h\sqrt{\frac{2}{\lambda} \frac{d_T + d_R}{d_T d_R}} \quad (3)$$

and depends on the obstruction depth h . The real and imaginary parts of $F(\nu)$ can be recalled as follows:

$$F(\nu) = C(\nu) + jS(\nu)$$

The Fresnel integral can be computed by numerical calculation, however [39] provides a simple way to compute an approximate result.

Obstruction

When an obstacle cuts through a transmission path, the simplest obstruction model consists in applying a constant loss L during the shadowing window, resulting in a sharp transition between an obstructed and an unobstructed path. The obstruction loss is generally computed based on the absorption properties of the obstacle. Depending on the model assumptions, an obstructed path may be completely removed from the scenario. Its simplicity makes this model desirable in terms of computational and implementation complexity, so that it has often been chosen for end-to-end network simulations [40]–[42]. Unfortunately, the unrealistic sharp drop not only yields imprecise results, but can also affect some beam-tracking algorithms, which are of the utmost importance when it comes to mmWave communication.

METIS

The Mobile and wireless communications Enablers for the Twenty-twenty Information Society (METIS) channel model [21] provides a simplified method to account for the diffraction contribution at mmWave frequencies. The screen is assumed to be vertical and perpendicularly oriented with respect to the considered ray segment in the projection from above. The diffraction loss is modeled using a KED model for the four edges of the screen as:

$$L = -20 \log_{10}(1 - (l_{h1} + l_{h2})(l_{w1} + l_{w2})) \quad [\text{dB}] \quad (4)$$

where l_{hi} and l_{wi} are the Single Knife-Edge Diffraction (SKED) at edge i , corresponding to the height h and the width w of the obstacle. The loss of each single edge is provided by:

$$l_i = \frac{\text{atan}\left(\pm \frac{\pi}{2} \sqrt{\frac{\pi(d_{T,i} + d_{R,i} - r)}{\lambda}}\right)}{\pi} \quad (5)$$

where, as shown in Fig. 1, $d_{T,i}$ and $d_{R,i}$ are the distances between the nodes and edge i of the screen, and r is the distance between the TX and the RX. If the link is NLoS, then each contribution is taken as positive, whereas for LoS condition, only the farthest edge from the link provides a positive contribution.

Double Knife-Edge Diffraction (DKED)

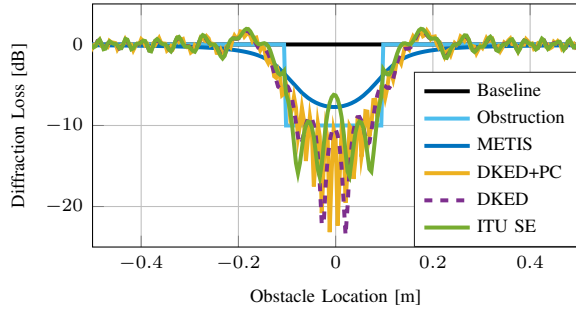
This model [43] computes the SKED from the screen edges evaluating both amplitudes and phases. Since only the lateral edges are considered for the KED, the interaction of the obstacle with the propagating waves is that of a vertical stripe of infinite vertical extent. The SKED for edge i can be computed as:

$$l_i = \frac{1+j}{2} \left[\left(\frac{1}{2} - C(\nu_i) \right) - j \left(\frac{1}{2} - S(\nu_i) \right) \right] \quad (6)$$

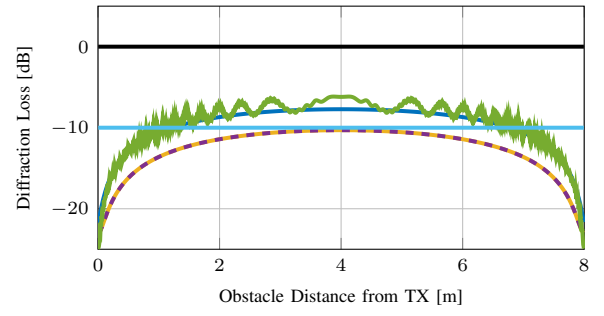
and then, this model computes the superposition of each contribution to obtain the diffraction loss:

$$L = -20 \log_{10}(|l_1 + l_2|) \quad [\text{dB}] \quad (7)$$

Besides, as the *Semi-empirical ITU* model, it provides a valid solution even for non-orthogonal obstacles, and thus can be exploited for a larger variety of obstacles.



(a) Models at 60 GHz



(b) Different obstacle's distance

Fig. 2: Comparison between the implemented models using a carrier frequency of 60 GHz.

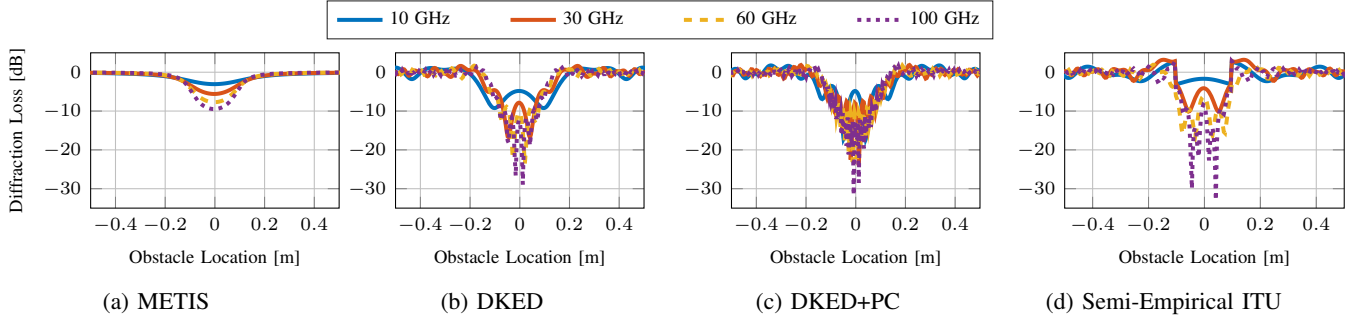


Fig. 3: Comparison of the implemented models at different frequencies.

Double Knife-Edge Diffraction with Phase Correction (DKED+PC)

In [43], the authors present also a modified version of the DKED. Namely, the SKED is computed for the two contributions (front and back of the body) as described by Eq. (6) for the DKED model. Additionally, this method takes into account the phase shift of the diffracted rays path when combining the two contributions.

$$L = -20 \log_{10} \left(\left| l_1 \cdot e^{-j \frac{2\pi \Delta d_1}{\lambda}} + l_2 \cdot e^{-j \frac{2\pi \Delta d_2}{\lambda}} \right| \right) \quad [\text{dB}] \quad (8)$$

where Δd_i is the length of the i -th diffracted ray. The model is presented and calibrated for ultra-wideband measurements between 4 and 10 GHz. However, its analytical derivation is based on the Fresnel diffraction theory, that holds also for higher frequencies, as reported in [7].

ITU-R P.526-15

The International Telecommunication Union (ITU) provides guidelines on the modeling of the diffraction in [39]. Based on the Uniform Theory of Diffraction (UTD) and on high-precision measurements, two approximations are given for estimating the minimum and the average diffraction loss. Furthermore, a Semi-Empirical method (ITU SE) is derived for thin rectangular screens, that exhibits the rapid fluctuations of the field strength due to the constructive and destructive interference of the diffraction from the edges. This method can be used also for non-orthogonal obstacles. Moreover, with reasonable accuracy, it does not require the Fresnel integral to be solved. Both models can be applied when the wavelength is fairly small in relation to the size of the obstacles, which is the case when considering human-size blockers at mmWave frequencies. The mathematical details of this method are reported in [39].

V. RESULTS

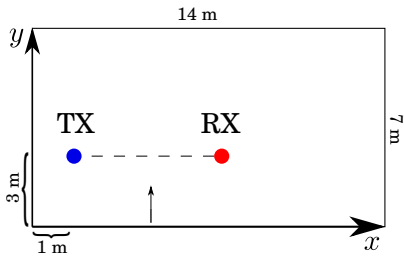
In this section, we present a set of results obtained using the *Blockage Manager*, to showcase the framework and offer some insight on the impact of blockage modeling on network simulations, and to compare the different diffraction models. First, in Sec. V-A, we will show their general behavior as directly described by the equations, thus considering the effect that the obstacle has when passing through the direct ray between transmitter and receiver.

Then, Sec. V-B will consider a more realistic *static* scenario, where transmitter and receiver are still fixed but placed in a room, and reflections, computed using a ray-tracer, also interact with the moving obstacle.

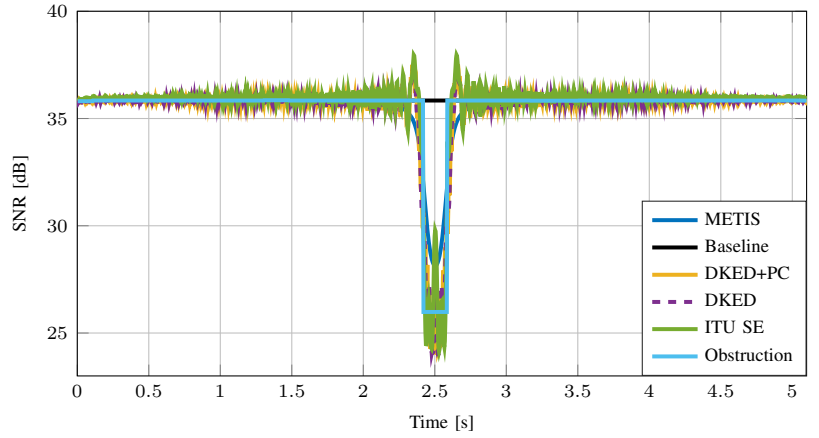
Finally, in Sec. V-C a more complex *dynamic* scenario is evaluated, where we consider an access point placed on the ceiling of a room and a user moving away from it. In this case, multiple obstacles move in the scenario, to make the simulation even more realistic.

All the scenarios but one consider the obstacle(s) passing through the LoS ray to better highlight the effect of the diffraction on the received power. As detailed in the following, we consider also the case where the obstacles do not intercept the main ray, but only the reflected ones, to show that diffraction is relevant also in this situation. For this work, we consider an (orthogonal-rectangular) thin screen, which provides a simplified yet realistic representation of the human body, according to measurements [7], [43] and standards [21], [39]. The obstruction loss is set to 10 dB, obtained by averaging the mean loss of the considered diffraction models.

First, the *qd-realization* traces are imported in the *Blockage Manager*, that applies the diffraction loss to the rays according to the obstacle configuration. Link-layer simulations are then run on the traces using the same custom MATLAB simulator as in [6], [44], to observe the blockage effect on the SNR. However, given that the format of the output traces of



(a) Static scenario.



(b) Max reflection order: 2

Fig. 4: Static scenario including second-order reflections.

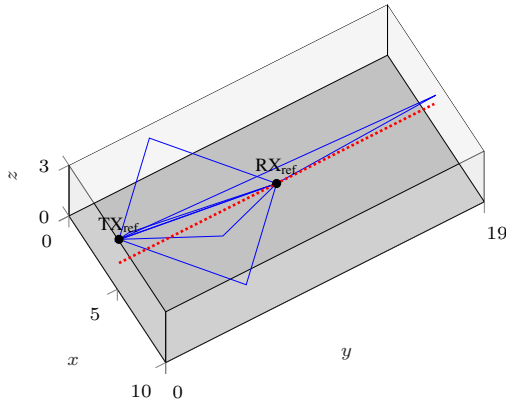


Fig. 5: Dynamic scenario

the *Blockage Manager* is the same as that of *qd-realization*, they are compatible with other simulators such as Network Simulator 3 (ns-3) [45]. The main parameters used for link-level simulations are listed in Table I. Beamforming at both the transmitter and the receiver is achieved using an antenna array with omnidirectional antenna elements and $\lambda/2$ element spacing.

A. Model Comparison

All implemented models have their own distinct characteristics derived by their formulations. To give the reader an idea of their behavior, we show a set of key comparisons for these models in scenarios of interest.

We first consider a TX at 1.6 m height, and a RX at the same height placed 8 m away from the transmitter. An obstacle of size 0.2×1.7 m passes perpendicularly halfway between TX and RX, blocking the LoS between the two nodes. To highlight the effect of the models, we only process the direct ray, normalizing the received power to obtain the diffraction loss. Fig. 2a shows the losses of the different models at a 60 GHz carrier frequency.

TABLE I: Simulation parameters

TX Antenna	8×8	RX Antenna	4×4
Antenna Spacing	$\frac{\lambda}{2}$	Antenna Element	omni-directional
Carrier Frequency	60 GHz	Bandwidth	2.16 GHz
TX Power	20 dBm	Noise Figure	10 dB

In particular, the difference between the simple obstruction and the more complex diffraction models can be clearly observed. Complex physics-based models, in fact, show an oscillatory behavior before and after the obstacle even intercepts the LoS, due to its effect on the surrounding propagation environment, with peaks of almost 2 dB. Furthermore, within the blockage region, very sharp deep fades affect the channel with over 10 dB extra losses, due to destructive interference among the rays curving around the obstacle. This phenomenon, together with the high obstruction loss, can make channel estimation and adaptation harder, thus further reducing the communication efficiency in the presence of obstacles. It is also possible to observe that different models have different average obstruction losses, making us question which one, if any, is close to the real-world measurements.

Instead, Fig. 2b shows what happens for the different models when the same obstacle moves starting close to the TX and moving towards the RX, always obstructing the direct path between the two. For all diffraction models, the distance between the obstacle and the nodes is taken into account when modeling its effect on the channel. The figure shows a symmetric behavior, justified by the symmetry of wireless propagation, and all curves follow approximately the same trend. Specifically, the loss tends to be higher when the obstacle is close to one of the nodes, and is lowest when the obstacle is exactly in the middle, a trend that is observed irrespective of the distance between TX and RX. Intuitively, in fact, rays that need a sharper turn to surpass the obstacle (i.e., when the obstacle is close to one of the nodes) lose more energy than rays that need a shallower turn (i.e., when the obstacle is farthest). A different explanation can be given by thinking about the apparent size of the obstacle, as seen from one of the nodes. The same obstacle has a different apparent size depending on how far it is from its observer, where closer objects appear larger than farther objects and thus result in a deeper shadow.

Finally, it is important to remember that these models heavily depend on the carrier frequency. In fact, in general higher frequencies will present sharper and larger losses, due to the larger electrical size of the obstacle with respect to the wavelength. The short wavelength will also be more prone to creating constructive and destructive interference between the rays bending around the obstacle, creating deeper and

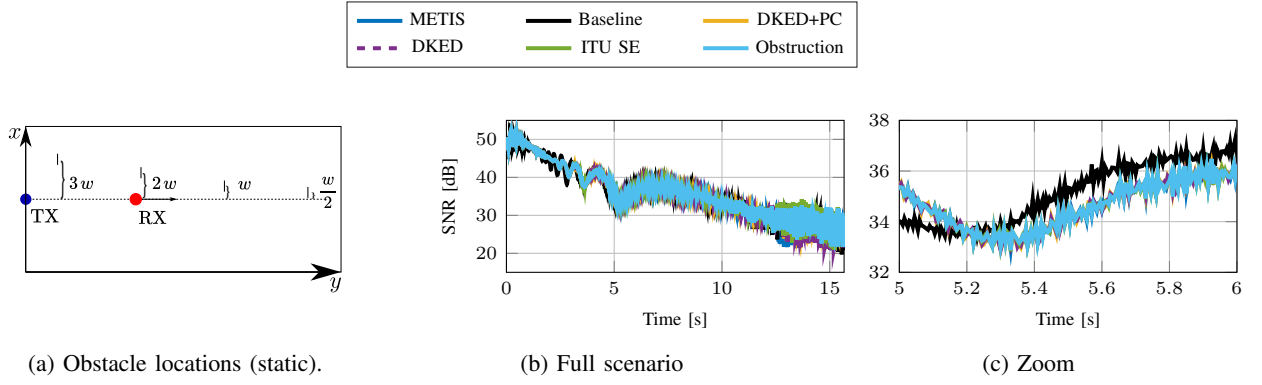


Fig. 6: Dynamic scenario with 4 static obstacles.

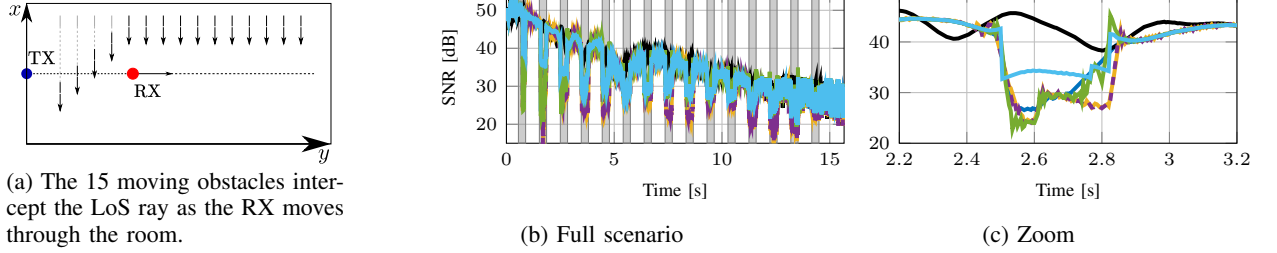


Fig. 7: Dynamic scenario with 15 dynamic obstacles.

more frequent loss peaks. Longer wavelength, instead, will be able to more easily bend around an obstacle, greatly reducing the obstruction losses. These results can also be observed in Fig. 3.

B. Static Scenario

We tested our framework in a scenario inspired by [7]. Specifically, two static nodes are placed in positions $p_1 = (1, 3, 1.6)$ and $p_2 = (9, 3, 1.6)$ within a $14 \times 7 \times 3$ m³ room, as shown in Fig. 4a. We simulated the channel with *qd-realization* [9], an open-source ray-tracing software for mmWave propagation, considering up to second-order reflections.

We then imported the channel trace into the *Blockage Manager* software, configuring an orthogonal-rectangular screen moving from $p_{\text{start}} = (5, 0, 0)$ upwards at 1.2 m/s, and sampled the channel every 3.4 ms for 1500 samples, for a total of about 5 s of simulation time. We considered a thin screen with a width of 20 cm and a height of 1.7 m, in an attempt to emulate the size of the human body.

Fig. 4b reports the SNR observed by the receiving node. As the obstacle crosses through the LoS, the SNR decreases rapidly, showing a behavior similar to that described in Sec. V-A both in shape and in amplitude. Specifically, observing a diffraction loss so close to the one presented in Fig. 2 highlights how the LoS ray carries the great majority of the signal power to the receiver, while the reflected ray can not compensate for the diffraction loss caused by the blocker. On the other hand, while the average loss is similar to the one described in Sec. V-A, the deepest fades are mitigated by secondary reflected rays carrying far less power. Namely, the troughs observed in most of the diffraction models often overestimate the fade depth [7]. However, a complete channel simulation, where the transceivers and the obstacles are immersed in a realistic three-dimensional environment, tends to average them out, reducing the overall overshooting.

C. Dynamic Scenario

For this scenario, a different room is considered: the length and width are respectively equal to 19 m and 10 m, whereas the height is 3 m as described in Fig. 5.

Although the environment, a rectangular room, is similar to the previous one, in this case the receiver is not fixed and the two nodes are not at the same height. Indeed the transmitter has a fixed position in $p_1 = (5, 0.1, 2.9)$ and the receiver starts from a position right below the transmitter, $p_{\text{start}} = (5, 0.1, 1.5)$, and moves away from it at 1.2 m/s for about 15.7 s, reaching the position $p_{\text{final}} = (5, 18.9, 1.5)$ next to the farthest wall from the TX position. The total number of samples is 3133, achieved using a sampling period of 5 ms. Following the results from [6], we simulated up to second-order reflections, and excluded rays less powerful than the most prominent one by more than 40 dB. These parameters were shown to yield a good balance between computational effort and accuracy of results. We then imported the results into the *Blockage Manager* software with two different obstacle settings.

In the first scenario, reported in Fig. 6a, 4 static obstacles of size 0.4×1.7 m² are considered, none of them blocking the direct ray. The obstacles are placed at decreasing distances from the LoS, specifically in $p_1 = (5.2, 15.14, 0)$, $p_2 = (5.8, 7.62, 0)$, $p_3 = (5.4, 11.38, 0)$, and $p_4 = (6.2, 3.86, 0)$.

As shown in Fig. 6, although the obstacles do not create strong or sudden effects on the received power, they still play an important role in the total received power, showing differences with respect to the baseline of up to 8.2 dB. On the other hand, as the RX passes by the first three obstacles, all models behave almost indistinguishably from each other, with an absolute error of at most 1.6 dB with respect to the simple obstruction model. On the contrary, the diffraction introduced by the last and closest screen is significant, with the SNR of the diffraction models presenting a difference of about 5 dB

from that of the obstruction model. This justifies our design choice of setting a distance threshold on the diffraction model, so that obstacles far enough from the ray will not affect it, making it sufficient to only model the most significant effects of the diffraction. Similarly, we also allow the user to fall back to a simpler obstruction model for secondary or less powerful rays, which have a much smaller effect on the total received power.

Finally, in the second scenario we consider 15 obstacles traversing the room at regular intervals, as represented in Fig. 7a. The results in Fig. 7 show all the effects discussed so far in the previous sections, combined in a more complex and realistic scenario. In particular, it is possible to observe that (i) all models behave as expected during obstruction (highlighted in gray), (ii) obstacles affect the channel also when not directly blocking the LoS, (iii) constructive interference before and after obstruction can actually be very significant, even overshooting the baseline, (iv) using a constant obstruction loss does not represent well the complex interaction between transceivers and obstacles, (v) when the receiver reaches the other side of the room, and with multiple rays having similar power to the direct path, obstruction is less severe and small scale fading is actually the main concern.

VI. CONCLUSIONS

In this paper we presented a novel open source tool, the *Blockage Manager*, to model the diffraction by dynamic obstacles in RT traces. Namely, the software post-processes the output from a ray-tracer, allowing the user to introduce an arbitrary number of obstacles in the simulation, and modeling their interactions with the rays choosing from a number of diffraction models. The potential of the software was showcased with simple yet insightful network simulations, which already provided interesting results. We hope that this tool lays the foundations for more accurate, large-scale studies on the effects of blockage on mmWave networks.

Comparison with real-world data is an essential step to validate the framework. A more precise calibration of the diffraction models against measurements is currently being considered, and we plan to provide a calibration toolbox as an additional module for the framework.

Future steps will also focus on making the *Blockage Manager* able to describe a much wider variety of scenarios, introducing new obstacles and diffraction models. For instance, a foliage model could be implemented to increase the accuracy in outdoor environments where the signal propagates through trees and vegetation. Furthermore, UTD may be considered as a more general approach to model the diffraction, including obstacles of arbitrary shape and dimension.

Finally, a full stack analysis of a real scenario with accurate obstacle models is essential to understand more precisely the actual effect of multiple, dynamic obstacles on the final user experience in different practical situations.

REFERENCES

- [1] T. S. Rappaport, S. Sun, R. Mayzus, H. Zhao, Y. Azar, K. Wang, G. N. Wong, J. K. Schulz, M. Samimi, and F. Gutierrez, "Millimeter wave mobile communications for 5G cellular: It will work!" *IEEE Access*, vol. 1, pp. 335–349, 2013.
- [2] S. Rangan, T. S. Rappaport, and E. Erkip, "Millimeter-wave cellular wireless networks: Potentials and challenges," *Proceedings of the IEEE*, vol. 102, no. 3, pp. 366–385, Mar. 2014.
- [3] S. Deng, G. R. MacCartney, and T. S. Rappaport, "Indoor and outdoor 5G diffraction measurements and models at 10, 20, and 26 GHz," in *IEEE Global Communications Conference (GLOBECOM)*, Dec. 2016.
- [4] I. A. Hemadeh, K. Satyanarayana, M. El-Hajjar, and L. Hanzo, "Millimeter-wave communications: Physical channel models, design considerations, antenna constructions, and link-budget," *IEEE Communications Surveys and Tutorials*, vol. 20, no. 2, pp. 870–913, Second Quarter 2018.
- [5] M. Lecci, P. Testolina, M. Giordani, M. Polese, T. Ropitault, C. Gentile, N. Varshney, A. Bodi, and M. Zorzi, "Simplified Ray Tracing for the Millimeter Wave Channel: A Performance Evaluation," in *Information Theory and Applications Workshop (ITA)*, San Diego, CA, USA, Feb. 2020.
- [6] M. Lecci, P. Testolina, M. Polese, M. Giordani, and M. Zorzi, "Accuracy Versus Complexity for mmWave Ray-Tracing: A Full Stack Perspective," *IEEE Transactions on Wireless Communications*, vol. 20, no. 12, pp. 7826–7841, Dec. 2021.
- [7] A. Bhardwaj, D. Caudill, C. Gentile, J. Chuang, J. Senic, and D. G. Michelson, "Geometrical-empirical channel propagation model for human presence at 60 GHz," *IEEE Access*, vol. 9, pp. 38 467–38 478, 2021.
- [8] G. R. MacCartney, S. Deng, S. Sun, and T. S. Rappaport, "Millimeter-wave human blockage at 73 GHz with a simple double knife-edge diffraction model and extension for directional antennas," in *IEEE 84th Vehicular Technology Conference (VTC-Fall)*, Sep. 2016, pp. 1–6.
- [9] wigig-tools, "qd-realization," <https://github.com/signetlabdel/qd-realization/tree/feature/power-threshold>, open-source ray-tracer implementation.
- [10] T. Bai and R. W. Heath, "Coverage and rate analysis for millimeter-wave cellular networks," *IEEE Transactions on Wireless Communications*, vol. 14, no. 2, pp. 1100–1114, Feb. 2015.
- [11] J. G. Andrews, T. Bai, M. N. Kulkarni, A. Alkhateeb, A. K. Gupta, and R. W. Heath, "Modeling and analyzing millimeter wave cellular systems," *IEEE Transactions on Communications*, vol. 65, no. 1, pp. 403–430, Jan. 2017.
- [12] P. Ferrand, M. Amara, S. Valentin, and M. Guillaud, "Trends and challenges in wireless channel modeling for evolving radio access," *IEEE Communications Magazine*, vol. 54, no. 7, pp. 93–99, Jul. 2016.
- [13] 3GPP, "Study on channel model for frequencies from 0.5 to 100 GHz," 3rd Generation Partnership Project (3GPP), Technical Report (TR) 38.901, Jun. 2018, version 15.0.0.
- [14] M. Gapeyenko, V. Petrov, D. Moltchanov, S. Andreev, Y. Koucheryavy, M. Valkama, M. R. Akdeniz, and N. Himayat, "An Analytical Representation of the 3GPP 3D Channel Model Parameters for MmWave Bands," in *Proceedings of the 2nd ACM Workshop on Millimeter Wave Networks and Sensing Systems*, ser. mmNets '18. New Delhi, India: Association for Computing Machinery, 2018, p. 33–38. [Online]. Available: <https://doi.org/10.1145/3264492.3264498>
- [15] T. Zugno, M. Polese, N. Patriciello, B. Bojović, S. Lagen, and M. Zorzi, "Implementation of a Spatial Channel Model for Ns-3," in *ACM Workshop on Ns-3 (WNS3)*, Gaithersburg, MD, USA, Jun. 2020.
- [16] M. Lecci, M. Polese, C. Lai, J. Wang, C. Gentile, N. Golmie, and M. Zorzi, "Quasi-Deterministic Channel Model for mmWaves: Mathematical Formalization and Validation," in *IEEE Global Communications Conference (GLOBECOM)*, Taipei, Taiwan, Dec. 2020.
- [17] V. Degli-Esposti, F. Fuschini, E. M. Vitucci, M. Barbiroli, M. Zoli, L. Tian, X. Yin, D. A. Dupleich, R. Müller, C. Schneider, and R. S. Thomä, "Ray-tracing-based mm-Wave beamforming assessment," *IEEE Access*, vol. 2, pp. 1314–1325, 2014.
- [18] J. McKown and R. Hamilton, "Ray tracing as a design tool for radio networks," *IEEE Network*, vol. 5, no. 6, pp. 27–30, Nov. 1991.
- [19] K. Schuler, D. Becker, and W. Wiesbeck, "Extraction of virtual scattering centers of vehicles by ray-tracing simulations," *IEEE Transactions on Antennas and Propagation*, vol. 56, no. 11, pp. 3543–3551, Nov. 2008.
- [20] M. Ghaddar, L. Talbi, T. A. Denidni, and A. Sebak, "A conducting cylinder for modeling human body presence in indoor propagation channel," *IEEE Transactions on Antennas and Propagation*, vol. 55, no. 11, pp. 3099–3103, Nov. 2007.
- [21] "METIS Channel Models," Deliverable D1.4, Feb. 2015.
- [22] J. Medbo and F. Harrysson, "Channel modeling for the stationary UE scenario," in *7th European Conference on Antennas and Propagation (EuCAP)*, Gothenburg, Sweden, Apr. 2013.
- [23] M. D. Casciato, "Radio wave diffraction and scattering models for wireless channel simulation," Ph.D. dissertation, University of Michigan, 2001.
- [24] D. Prado-Alvarez, S. Inca, D. Martín-Sacristán, and J. F. Monserrat, "Millimeter-wave human blockage model enhancements for directional antennas and multiple blockers," *IEEE Communications Letters*, vol. 25, no. 9, pp. 2776–2780, Sep. 2021.
- [25] C. Slezak, M. Zhang, M. Mezzavilla, and S. Rangan, "Understanding End-to-End Effects of Channel Dynamics in Millimeter Wave 5G New Radio," in *IEEE 19th International Workshop on Signal Processing Advances in Wireless Communications (SPAWC)*, 2018, pp. 1–5.

- [26] M. Jacob, S. Priebe, A. Maltsev, A. Lomayev, V. Erceg, and T. Kurner, "A ray tracing based stochastic human blockage model for the IEEE 802.11ad 60 GHz channel model," in *5th European Conference on Antennas and Propagation (EuCAP)*, Rome, Italy, Apr. 2011.
- [27] A. Maltsev *et al.*, "Channel models for 60 GHz WLAN systems," 09/0334r8, IEEE Task Group ad (TGad), Tech. Rep., May 2010.
- [28] M. Zhang, M. Polese, M. Mezzavilla, J. Zhu, S. Rangan, S. Panwar, and M. Zorzi, "Will TCP Work in mmWave 5G Cellular Networks?" *IEEE Communications Magazine*, vol. 57, no. 1, pp. 65–71, January 2019.
- [29] M. Polese, M. Mezzavilla, S. Rangan, and M. Zorzi, "Mobility Management for TCP in MmWave Networks," in *1st ACM Workshop on Millimeter-Wave Networks and Sensing Systems (mmNets)*, ser. mmNets '17, Snowbird, Utah, USA, Oct. 2017.
- [30] M. Polese, M. Mezzavilla, M. Zhang, J. Zhu, S. Rangan, S. Panwar, and M. Zorzi, "milliProxy: A TCP proxy architecture for 5G mmWave cellular systems," in *51st Asilomar Conference on Signals, Systems, and Computers*, 2017, pp. 951–957.
- [31] M. Polese, R. Jana, and M. Zorzi, "TCP in 5G mmWave networks: Link level retransmissions and MP-TCP," in *IEEE Conference on Computer Communications Workshops (INFOCOM WKSHPS)*, 2017, pp. 343–348.
- [32] —, "TCP and MP-TCP in 5G mmWave Networks," *IEEE Internet Computing*, vol. 21, no. 5, pp. 12–19, Sep. 2017.
- [33] M. Mezzavilla, M. Zhang, M. Polese, R. Ford, S. Dutta, S. Rangan, and M. Zorzi, "End-to-end simulation of 5G mmWave networks," *IEEE Communications Surveys and Tutorials*, vol. 20, no. 3, pp. 2237–2263, Third Quarter 2018.
- [34] Y. Ren, W. Yang, X. Zhou, H. Chen, and B. Liu, "A survey on TCP over mmWave," *Computer Communications*, vol. 171, pp. 80–88, Apr. 2021.
- [35] I. Khan, M. Ghoshal, S. Aggarwal, D. Koutsonikolas, and J. Widmer, "Multipath TCP in Smartphones Equipped with Millimeter Wave Radios," in *15th ACM Workshop on Wireless Network Testbeds, Experimental Evaluation and Characterization (WiNTECH)*, New Orleans, LA, USA, Jan. 2022.
- [36] C. Lee, S. Song, H. Cho, G. Lim, and J.-M. Chung, "Optimal Multipath TCP Offloading Over 5G NR and LTE Networks," *IEEE Wireless Communications Letters*, vol. 8, no. 1, pp. 293–296, Feb. 2019.
- [37] A. Meurer, C. P. Smith, M. Paprocki, O. Čertík, S. B. Kirpichev, M. Rocklin, A. Kumar, S. Ivanov, J. K. Moore, S. Singh, T. Rathnayake, S. Vig, B. E. Granger, R. P. Muller, F. Bonazzi, H. Gupta, S. Vats, F. Johansson, F. Pedregosa, M. J. Curry, A. R. Terrel, v. Roučka, A. Saboo, I. Fernando, S. Kulal, R. Cimrman, and A. Scopatz, "SymPy: symbolic computing in python," *PeerJ Computer Science*, vol. 3, p. e103, Jan. 2017. [Online]. Available: <https://doi.org/10.7717/peerj-cs.103>
- [38] S. Gillies *et al.*, "Shapely: manipulation and analysis of geometric objects," 2007–. [Online]. Available: <https://github.com/shapely/shapely>
- [39] ITU-R, "Propagation by diffraction," Recommendation ITU-R P.526-15, Oct. 2019.
- [40] R. Ford, M. Zhang, S. Dutta, M. Mezzavilla, S. Rangan, and M. Zorzi, "A Framework for End-to-End Evaluation of 5G MmWave Cellular Networks in Ns-3," in *Proceedings of the ACM Workshop on Ns-3 (WNS3)*, Seattle, WA, USA, Jun. 2016.
- [41] H. Assasa and J. Widmer, "Implementation and Evaluation of a WLAN IEEE 802.11ad Model in Ns-3," in *Proceedings of the Workshop on Ns-3 (WNS3)*, Seattle, WA, USA, Jun. 2016.
- [42] —, "Extending the IEEE 802.11ad Model: Scheduled Access, Spatial Reuse, Clustering, and Relaying," in *Proceedings of the Workshop on Ns-3 (WNS3)*, Porto, Portugal, Jun. 2017.
- [43] J. Kunisch and J. Pamp, "Ultra-wideband double vertical knife-edge model for obstruction of a ray by a person," in *IEEE International Conference on Ultra-Wideband*, Hannover, Germany, Sep. 2008.
- [44] P. Testolina, M. Lecci, M. Polese, M. Giordani, and M. Zorzi, "Scalable and accurate modeling of the millimeter wave channel," in *International Conference on Computing, Networking and Communications (ICNC)*, Feb. 2020, pp. 969–974.
- [45] T. R. Henderson, M. Lacage, G. F. Riley, C. Dowell, and J. Kopena, "Network simulations with the ns-3 simulator," vol. 14, no. 14, 2008, p. 527.